Printing of Hydrophobic Materials in Fumed Silica Nanoparticle Suspension

Yifei Jin[1], Kaidong Song[1], Nevada Gellermann[2], Yong Huang[1,3,4,]*

[1]Department of Mechanical and Aerospace Engineering, University of Florida, Gainesville, FL, 32611, USA.

[2]Department of Physics, University of Florida, Gainesville, FL, 32611, USA.

[3]Department of Materials Science and Engineering, University of Florida, Gainesville, FL 32611, USA.

[4]Department of Biomedical Engineering, University of Florida, Gainesville, FL 32611, USA.

*Corresponding author, Department of Mechanical and Aerospace Engineering, University of Florida, Gainesville, FL 32611, USA

Phone: 001-352-392-5520, Fax: 001- 352-392-7303, Email: yongh@ufl.edu.

KEYWORDS: 3D printing; fumed silica-mineral oil suspension; solid-liquid transition; hydrophobic liquid material; interfacial tension

ABSTRACT

Freeform three-dimensional (3D) printing of functional structures from liquid hydrophobic build materials is of great significance and widely used in various fields such as soft robotics and microfluidics. In particular, a yield-stress support bath-enabled 3D printing methodology has been emerging to fabricate complex 3D structures. Unfortunately, the reported support bath

materials are either hydrophobic or not versatile enough for the printing of a wide range of hydrophobic materials. The objective of this study is to propose a fumed silica nanoparticle-based yield-stress suspension as a hydrophobic support bath to enable 3D extrusion printing of various hydrophobic ink materials in a printing-then-solidification fashion. Hydrophobic ink is freeform deposited in a hydrophobic fumed silica-mineral oil suspension and remains its shape during printing; it is not cured until the whole structure is complete. Various hydrophobic inks including polydimethylsiloxane (PDMS), SU-8 resin, and epoxy-based conductive ink are printed into complex 3D structures in the fumed silica-mineral oil bath and then cured using relevant cross-linking mechanisms, even at a temperature as high as 90°C, to prove the feasibility and versatility of the proposed printing approach. In addition, the deposited feature can easily reach a much better resolution such as 30 μm for PDMS filaments due to the negligible interfacial tension effect.

1. INTRODUCTION

Various materials have been developed and utilized to fabricate functional structures such as soft robotics/actuators [1-3], electronic components/devices [4-6], and mechanical parts [7, 8], to name a few, for various applications. The emergence of three-dimensional (3D) printing [9] provides a powerful tool for on-demand fabrication of complex 3D functional structures. For freeform 3D printing of functional structures, extrusion [1-6, 10], sometimes known as direct ink writing, is one of the commonly used strategies due to its easy implementation, high efficiency and wide range of printable materials. During extrusion printing, functional ink materials must have either rapid solidification properties [1, 3] or self-supporting properties [11-14] to keep the shape as extruded, which constrains the selection of printable materials. To overcome this challenge, a yield-stress

support bath-assisted printing-then-solidification extrusion strategy [15] has been emerging in recent years as an alternative methodology to print functional materials. During printing, a yield-stress support bath is utilized to temporarily hold a printed 3D structure *in situ*, which is not cured until the whole structure is complete.

To date, various hydrophilic yield-stress support bath materials such as granular microgels [16-18], Laponite nanoclay particles [15, 19-20], and gelatin particles [21] have been investigated for extrusion printing of aqueous materials. When a bath material is hydrophilic, the interfacial tension effect may prevent extrusion printing of fine features from hydrophobic liquids as seen from the Plateau-Rayleigh instability principle. If printing in a hydrophilic bath, printed continuous filaments of hydrophobic functional ink materials may easily result in discontinuous segments or droplets. For hydrophobic support bath-based extrusion printing, a self-assembled micro-organogel bath was investigated to print silicone structures [22]. However, this micro-organogel bath is sensitive to temperature changes and loses its supporting function if the working temperature is higher than 60 °C, constraining its applications for printing of high cross-linking/solidification temperature ink materials. Therefore, it calls for a new hydrophobic support bath material for hydrophobic material printing.

Ideally, a support bath material for hydrophobic ink printing must have following properties: 1) it should be a structured fluid with a short response time thixotropic property and have a solid-liquid transition upon a certain yield stress, which enables it to easily and rapidly transit between liquid and solid states upon different shear stress conditions, 2) it should be hydrophobic, which may mitigate the interfacial tension effect during printing, and 3) it should have thermal stability and UV transparency to facilitate 3D printing of various hydrophobic functional inks with different cross-linking mechanisms.

The objective of this study is to investigate a fumed silica-mineral oil system as the support bath, in which fumed silica powders are suspended in mineral oil to prepare a yield-stress suspension. Since the hydrophobic mineral oil is used as the solvent, the interfacial tension between the support bath material and hydrophobic ink materials is much lower than that in aqueous solvent-based support baths, which makes it feasible to fabricate complex 3D functional structures with a much better resolution from hydrophobic liquids. In addition, due to the inorganic nature of fumed silica nanoparticles and the relatively high boiling point of mineral oil (~ 220°C vs 140°C of silicone oil), the fumed silica-mineral oil support bath can endure a higher temperature range while maintaining a good yield-stress property for effective printing of thermally sensitive hydrophobic ink materials.

2. EXPERIMENTAL SECTION

2.1. Material preparation. Fumed silica nanoparticle suspension preparation. Commercial hydrophobic fumed silica Aerosil@R812 (Evonik, Parsippany, NJ) was used as the support bath material for various hydrophobic functional ink printing. Fumed silica nanoparticle suspensions were prepared by dispersing the appropriate amount of dry fumed silica powder in mineral oil (light, Sigma-Aldrich, St. Louis, MO) at room temperature. After continuous mixing for 90 min using an overhead stirrer (Thermo Fisher Scientific, Waltham, MA) at 500 rpm, the fumed silica nanoparticle suspensions were aged for at least one day. Before each use, the fumed silica nanoparticle suspensions were centrifuged using a centrifuge (5804R, Eppendorf, Hamburg, Germany) at 3000 rpm for 10 min to completely remove bubbles trapped in the suspensions. Specifically, 4.0%, 6.0% and 8.0% (w/v) fumed silica nanoparticle suspensions were used to characterize the rheological properties, UV transparency, and thermal stability of the suspensions.

For various hydrophobic ink printing studies, 6.0% (w/v) fumed silica nanoparticle suspension was used as the support bath.

Hydrophobic functional ink preparation. The PDMS (Sylgard 184, Dow Corning, Mildland, MI) ink was prepared by mixing the base agent with the curing agent using a glass rod at the volume ratio of 5:1 for 5 minutes. Before printing, PDMS ink was degassed using the centrifuge at 1500 rpm for 5 minutes to remove entrapped bubbles. The photosensitive SU-8 2050 (MicroChem, Westborough, MA), having a viscosity of 12,900 cP, was used as received to fabricate SU-8 structures. The commercial epoxy-based conductive ink (H22 EPO-TEK, TED PELLA, Redding, CA) was prepared by mixing the base agent with the hardener using a glass rod at the weight ratio of 100: 4.5 per the manufacturer's protocol and degassed using the centrifuge at 1500 rpm for 5 minutes to remove entrapped bubbles.

2.2. Characterization of fumed silica nanoparticle suspensions. Micro- and nano-scale structures of fumed silica nanoparticle suspensions were observed using both a scanning electron microscope (SEM) (SU5000 FE-VP SEM, Hitachi High Technologies America, Schaumburg, IL) and a transmission electron microscope (TEM) (Hitachi H7000 TEM, Hitachi High Technologies America, Schaumburg, IL). The fumed silica samples for SEM and TEM imaging were prepared by diluting 6.0% (w/v) fumed silica nanoparticle suspensions with 100% EtOH at the volume ratio of 1:1. Then the diluted fumed silica nanoparticle suspensions were sputter coated onto a plastic coverslip which was mounted onto a 25 mm carbon tab/25 mm stub for imaging. The SEM and TEM were operated at 5-10 kV and 100 kV, respectively.

Rheological properties of the fumed silica nanoparticle suspensions at different concentrations were measured using a rheometer (Anton Paar MCR 702, Ashland, VA) with a parallel plate measuring geometry (a diameter of 25.0 mm and a plate-to-plate gap distance of

1.0 mm). Steady shear rate sweeps were performed by varying the shear rate from 0.01 to 500 s^{-1} to determine the yield stress of the fumed silica nanoparticle suspensions. Frequency sweeps (frequency range: 0.05 ~ 10 Hz) were performed at a low strain of 1.0% for the fumed silica nanoparticle suspensions to explore the degree of fluid-like behavior. During transient step shear rate tests which were used to evaluate the thixotropic response time of the bath materials, fumed silica nanoparticle suspensions at different concentrations were pre-sheared at the shear rate of 10 s^{-1} for 120 seconds at the beginning and then the shear rate decreased to 0.01 s^{-1}. The viscosity variation was recorded during the subsequent 300 seconds.

The UV/Vis transparency of fumed silica nanoparticle suspensions at different concentrations was measured using a UV/Vis spectrophotometer (UV-1800, Shimadzu, Tokyo, Japan). The UV/visible light wavelength was swept from 200 nm to 1000 nm and the absorption of the light density passing through the fumed silica nanoparticle suspensions were recorded.

The thermal stability of the fumed silica nanoparticle suspensions was investigated using a rheometer (Anton Paar MCR 92, Ashland, VA) with a cone-plate measuring geometry (a diameter of 50 mm, a cone-to-plate gap distance of 100 μm, and a cone angle of 1.00°). Temperature sweeps were performed at a low strain of 1.0% for the fumed silica nanoparticle suspensions at different concentrations. The temperature increased from 25 °C to 100 °C with the increasing rate of 1 °C/10 s and the storage modulus at each temperature was measured.

2.3. Printing system and printing protocols. The extrusion system was a micro-dispensing pump machine (nScrypt-3D-450, nScrypt, Orlando, FL) and all the hydrophobic inks were printed in the 6.0% (w/v) fumed silica bath at room temperature. For PDMS printing, a 30 gauge (150 μm inner diameter and 12.70 mm length) dispensing tip (EFD Nordson, Vilters, Switzerland) and a 25 gauge (250 μm inner diameter and 25.40 mm length) dispensing tip (EFD

Nordson, Vilters, Switzerland) were used to print the microchips and octopus-like structures in the fumed silica support baths, respectively. The step distances were set as 200 μm and 250 μm, and the printing pressures were 1.38×10^5 Pa (20 psi) and 1.73×10^5 Pa (25 psi), respectively. The path speed for microchip printing was 1.00 mm/s and that for octopus printing was 3.00 mm/s. After printing, the fumed silica baths containing the printed PDMS structures were heated to 80°C for 40 minutes to solidify the structures, which were then harvested from the baths. For SU-8 printing, a 27 gauge (200 μm inner diameter and 12.7 mm length) dispensing tip (EFD Nordson, Vilters, Switzerland) was used to print SU-8 structures in the fumed silica bath with a step distance of 150 μm. The dispensing pressure was 2.06×10^5 Pa (30 psi) and the path speed was 0.50 mm/s. After printing, the deposited structure in the bath was exposed to UV light for 15 minutes for cross-linking and then baked at 90°C for 30 minutes for the complete curing of SU-8. For conductive ink printing, a 25 gauge (250 μm inner diameter and 12.70 mm length) dispensing tip (EFD Nordson, Vilters, Switzerland) was used to print different electronic components in the fumed silica bath with a step distance of 200 μm. Specifically, the dispensing pressure for inductor and battery anode/cathode set printing was 1.73×10^5 Pa (25 psi). The path speeds for inductor and battery anode/cathode set printing were 1.00 mm/s and 1.25 mm/s, respectively. After printing, the electronic components were kept in the bath for 10 days at room temperature for cross-linking.

Digital 3D models for the various printing applications herein were designed using SolidWorks (Dassault Systemes SolidWorks Corp., Waltham, MA), and the corresponding STL files were sliced by Slic3r (http://slic3r.ort) to generate the G-codes for 3D printing.

2.4. Observation and analysis of printed filaments/sheets. To observe filament printing process, a 20 gauge (610 μm inner diameter and 38.10 mm length) dispensing tip (EFD Nordson,

Vilters, Switzerland) was used to deposit PDMS base agent mixed with a scarlet powdered pigment (Pearl Ex, Jacquard, Healdsburg, CA) in the 6.0% (w/v) fumed silica bath with the path speed of 2.00 mm/s and the printing pressure of 1.03×10^5 Pa (15 psi). Images and videos from the bottom and side views were captured using a high speed camera (Fastcam SA5, Photron, San Diego, CA) with the frame rate of 250 fps (frame per second). To investigate the effects of path speed and support bath on the filament diameter, PDMS base agent mixed with the scarlet color dye was printed in the 4.0%, 6.0%, and 8.0% (w/v) fumed silica nanoparticle suspensions respectively with the increasing path speed from 0.5 mm/s to 10.0 mm/s and the morphology of the deposited filaments was imaged by an optical microscopy (EVOS, XL Core, Thermo Fisher Scientific, Waltham, MA). To investigate the effects of step distance on sheet thickness and roughness, a 27 gauge (200 μm inner diameter and 12.7 mm length) dispensing tip was used to print PDMS sheets (40.0 mm × 4.0 mm) using PDMS ink mixed with the red color dye in the 6.0% (w/v) fumed silica bath. The step distance increased from 100 μm to 225 μm with each interval of 25 μm, the printing pressure was 1.03×10^5 Pa (15 psi), and the path speed was 1.0 mm/s. After printing, the PDMS sheets were kept in the fumed silica bath for 24 hours at room temperature for solidification and then removed from the bath for measurement. The surface and cross-section of the PDMS sheets were imaged by the optical microscopy.

2.5. SU-8 gear testing. Functional testing of the printed SU-8 gear was performed using a home-made gear testing setup, which was composed of a mini electric motor (DC 1.5-6 V, 15000-16500 rpm), a supplementary gear, and an adjustable DC power supply (Model 1601, Maxtec, Chicago, IL). The voltage of the power supply increased from 0 V to 6 V and then decreased to 0 V in 30 seconds to finish a testing circle.

2.6. Resistance measurement and conductivity/electromagnetic property testing. Both casting and 3D printing were used to fabricate samples for resistance measurement. The home-made PDMS mold was used to cast the conductive samples with the dimensions of 20.0 mm × 7.5 mm × 1.2 mm. After filling the mold with epoxy-based conductive ink, the mold was submerged in a fumed silica bath for 10 days at room temperature to make the casting samples. The printed samples were fabricated per the aforementioned protocol with the same designed dimensions. The resistance was measured using a resistance meter (RM3544, Hioki, Nagano, Japan). Functional tests of the 3D printed conductive inductor were performed by connecting it in series with an adjustable DC power supply (Model 1601, Maxtec, Chicago, IL), several resistors and/or a LED light. By adjusting the voltage of the power supply, the brightness of the LED light or the magnetic field strength can be changed.

3. RESULTS AND DISCUSSION

3.1. Characterization of fumed silica suspension. The prepared transparent fumed silica-mineral oil suspension is illustrated in **Figure 1a**. Fumed silica nanoparticles are the basic unit to form fumed silica powders, which have spheroid-like shape with a diameter range from 5 to 50 nm as shown in **Figure 1a-1**. These nanoparticles have functional groups on the surface that interact with adjacent particles to form aggregates [23] with feature size of approximately 100-500 nm as shown in **Figure 1a-2** and even larger agglomerates as shown in **Figure 1a-3** as part of the fumed silica nanoparticle suspension (**Figure 1b-1**). To investigate the microstructures of the fumed silica-mineral oil suspension, morphological investigations are performed using a variable-pressure scanning electron microscopy (VP SEM). **Figure 1b-2** illustrates the morphology of solid-like fumed silica aggregates dispersed uniformly in mineral oil. The

spheroid-shaped particles as marked in **Figure 1b-2** present the fumed silica aggregates which are the fundamental unit to form the suspension. A fumed silica aggregate is composed of several fumed silica nanoparticles and the nanostructures of the fumed silica aggregates are imaged using transmission electron microscope (TEM) as shown in the inset of **Figure 1b-2**, in which the fumed silica nanoparticles can be observed with an average dimeter of around 20 nm. In the unstressed condition, numerous fumed silica aggregates cluster together to form the solid-state 3D networked microstructures as shown in **Figure 1b-1** and **b-2**, causing the solid-like behavior of the fumed silica nanoparticle suspension [24].

The functional groups on the surface of a fumed silica nanoparticle are usually determined by its processing method. Herein, the hydrophobic fumed silica nanoparticle suspension is utilized and the major functional groups found on the surface of nanoparticles are nonpolar carbon chains. When mixed with mineral oil, at static state the adjacent fumed silica agglomerates connect with each other by intermolecular bonding to form stable 3D networked microstructures (**Figure 1b-1**) due to Van der Waals force as shown in **Figure 1b-3**. The mineral oil molecules are entrapped inside the 3D networked microstructures. The fumed silica nanoparticle suspension presents a yield-stress property and behaves like solid. Under stressed condition the external shear stress may break up these bonds, and the stable 3D networked microstructures are disassembled back to the loose agglomerate debris [24] as shown in **Figure 1c**. This disrupted state microstructures of agglomerates enables the fumed silica nanoparticle suspension to behave like liquid. It is this solid-liquid transition of the fumed silica suspension upon yielding that makes fumed silica nanoparticle suspension easily switch between solid-like and liquid states and potentially be used as the support bath material for hydrophobic ink printing applications.

To further evaluate this suspension with solid-liquid transition can be used as a support bath material, the rheological properties of fumed silica nanoparticle suspension must be investigated. Thus, different rheological experiments are performed on fumed silica nanoparticle suspensions at different concentrations. First, the yield-stress property is investigated by steady sweeping fumed silica nanoparticle suspensions at different shear rates and measuring the shear stresses accordingly. The results are illustrated in **Figure 1d**. From **Figure 1d**, it is found that with the increase of shear rates, shear stresses of different concentration fumed silica nanoparticle suspensions also increase, while at low shear rate such as 0.01/s, the measured shear stress is still relatively high, which indicates the existence of yield stress in the fumed silica nanoparticle suspensions. This yield stress is the threshold between liquid and solid states of fumed silica nanoparticle suspensions: when the applied stress is higher than the yield stress, the suspension behaves like liquid, otherwise it behaves like solid. In addition, the yield stress increases with the fumed silica concentration as shown in **Figure 1d**. By fitting shear rate and stress data in the Herschel-Bulkley model: $\tau = \tau_0 + k\dot{\gamma}^n$, where τ is the shear stress, $\dot{\gamma}$ is the shear rate, τ_0 is the yield stress, k is the consistency index, and n is the flow index, the shear stresses of the fumed silica nanoparticle suspensions at the concentration of 4.0%, 6.0%, and 8.0% (w/v) can be calculated as approximately 4.0 Pa, 17.0 Pa, and 79.0 Pa, respectively. As a result, fumed silica nanoparticle suspensions with various yield-stress values can be achieved by varying the concentration.

Then, oscillatory tests are performed to investigate the relationship between shear moduli and frequency as shown in **Figure 1e**. From **Figure 1e**, it is found that for fumed silica nanoparticle suspensions with different concentrations the storage modulus is always higher than the loss modulus which indicates that fumed silica nanoparticle suspensions show solid-like behavior

under sheared condition, which can help maintain the deposited shape *in situ* during printing. Besides, both storage modulus and loss modulus increase with the increase of fumed silica concentration, which may affect the filament morphology in the support bath as reported in previous studies [19].

Finally, thixotropic time scale is investigated to evaluate the transition efficiency between liquid and solid states of the fumed silica nanoparticle suspensions, which determines whether deposited features can be effectively entrapped in the support bath during printing. **Figure 1f** illustrates the relationship between the viscosity change and responsive time. All the fumed silica nanoparticle suspensions are pre-sheared to a steadily sheared state, and then the shear rate decreases significantly. During this period, the viscosity change is recorded as shown in **Figure 1f**. From **Figure 1f**, due to the shear-thinning effect, the microstructures of fumed silica nanoparticles present a disrupted state and fumed silica nanoparticle suspensions have relatively low viscosity (from approximately 1 Pa·s to 10 Pa·s at different concentrations) during pre-shearing, however, after the shear rate is decreased dramatically, the microstructures of fumed silica nanoparticles rapidly recover to the solid-like 3D networked microstructures as shown in **Figure 1b-2**, resulting in significant increase in viscosity (from approximately 10^3 Pa·s to 10^4 Pa·s at different concentrations) in only 0.2s.

In addition to these basic rheological properties of support bath materials as aforementioned, a desired bath material should have light transparency, in particular, within the UV spectrum, and temperature robustness to facilitate the 3D printing of various hydrophobic inks with different cross-linking mechanisms since UV cross-linking and thermal cross-linking are two most commonly used cross-linking mechanisms to solidify liquid hydrophobic inks. Thus, the UV absorption of fumed silica nanoparticle suspensions at different concentrations is assessed

using the UV/Vis spectroscopy and the results are illustrated in **Figure 1g**. As seen from **Figure 1g**, it is found that in the wavelength range from 250 to 1000 nm, both UV and visible light can easily get through the fumed silica bath. In particular, the UV absorption in the wavelength range of a typical UV curing system (from 350 to 500 nm) is almost negligible as shown in the inset of **Figure 1g**. In addition, there is no pronounced difference of UV absorption between fumed silica nanoparticle suspensions at different concentrations, which verifies that fumed silica nanoparticle suspensions are the excellent support bath material to print UV curable hydrophobic inks.

After that, storage moduli of fumed silica nanoparticle suspensions at different temperatures are measured to evaluate the thermal stability and the results are shown in **Figure 1h**. As seen from **Figure 1h**, it is found that by increasing the temperature from room temperature (25 °C) to 100 °C, the storage moduli of fumed silica nanoparticle suspensions at different concentrations present negligible changes, which indicates that the solid-like 3D networked microstructure of fumed silica nanoparticle suspensions is not sensitive to temperature changes, resulting in the stable solid state of the suspensions at relative higher temperatures (at least up to 100 °C as investigated). Thus, fumed silica nanoparticle suspensions can be used as the support bath material for 3D printing of thermal cross-linkable hydrophobic inks.

3.2. Mechanism of fumed silica nanoparticle suspension-assisted fabrication approach. After characterizing the material properties of fumed silica nanoparticle suspension, we begin to use it as the support bath for 3D printing applications. The mechanism of fumed silica nanoparticle suspension-assisted 3D printing approach is illustrated in **Figure 2a**. When the nozzle moves in the fumed silica bath, the fumed silica aggregates around the nozzle tip has the shear stress higher than the yield stress. Thus, these aggregates turn into the disrupted state and

behave like liquid to entrap deposited features in the bath as well as to fill the crevasse behind the nozzle translation as shown in **Figure 2a-1**. In contrast, the fumed silica aggregates far away from the nozzle tip are in the unstressed condition, which allows the aggregates to recover to the stable 3D networked microstructures as shown in **Figure 2a-2**. As a result, the localized suspension behaves like a solid to stably hold the deposited features *in situ* for a long term.

3.3. Filament formation in fumed silica nanoparticle suspension. Since continuous filaments are the basic unit to form complex 3D structures during extrusion-based 3D printing, the filament formation in the fumed silica bath is investigated at the beginning. Polydimethylsiloxane (PDMS), a hydrophobic elastomer, has been widely used in various fields including soft robotics [2], wearable sensors [25], and organ-on-a-chip [26], to name a few, due to its transparency at optical frequencies, low autofluorescence, flexibility and biocompatibility [27]. However, the viscosity of PDMS is relatively low and the cross-linking period is comparatively long (approximately a few hours depending on the ambient temperature). Thus, it is a challenge to 3D print pure PDMS structures using conventional 3D printing techniques. Instead, molding is the most commonly used method to make PDMS structures [2, 25-26]. Herein, PDMS is selected as an exemplary hydrophobic ink to print filaments in the fumed silica bath. The printing process is illustrated in **Figure 2b-1** and **b-2** as well as **Movie M1**. From the figures and movie, we can find that a continuous filament with a uniform diameter can be easily deposited in the bath and stably held *in situ* due to the yield-stress property of fumed silica nanoparticle suspension as shown in **Figure 1d** and **f**. In addition, no crevasse behind the nozzle translation can be observed due to its short transition time between liquid and solid as shown in **Figure 1f**.

It is noted that printing PDMS in some aqueous support bath materials has been achieved in previous studies [17]. However, due to the hydrophobic property of PDMS, printed continuous

filaments, especially the filaments with small diameter, can easily break up into droplets. For example, a continuous PDMS filament (diameter of approximately 400 μm) can be printed in a hydrophilic Laponite RD bath as shown in **Supporting Information S1**, which gradually breaks up into segments in 2 minutes and finally into droplets in 10 minutes under the interfacial tension effect as shown in **Figure S1a**. Increasing filament diameter is one strategy to help maintain the filament morphology but may constrain the printing of PDMS structures with fine features in an aqueous support bath. In contrast, when printing in a fumed silica support bath, due to its hydrophobic property the interfacial tension between fumed silica nanoparticle suspension and liquid PDMS is comparatively low, which enables the PDMS filament (diameter of approximately 250 μm) to stably keep its original shape at liquid state (without solidification) for a long time (24 hours) as shown in **Figure S1b**.

To further explore the stability of continuous filaments in support bath materials, the interfacial tension between different solvents and liquid materials are measured and/or calculated [28] as shown in **Supporting Information S2** and **Movie M2**. As seen from **Figure S2a** and **b**, the interfacial tension between PDMS and aqueous solvent is relatively high (~42 mN/m) [17, 30], while the interfacial tension between PDMS and mineral oil is almost negligible (~ 0.21 mN/m). Based on Plateau-Rayleigh instability, the critical filament diameter (l_c) in a support bath is a function of interfacial tension (γ) and yield stress (τ_0): $l_c = \frac{\gamma}{\tau_0}$. When the filament diameter is higher than this critical value, the deposited filament can maintain its morphology, otherwise it breaks up into droplets under interfacial tension effect. Thus, the theoretically critical PDMS filament diameters in the hydrophobic fumed silica bath (τ_0 ~ 20 Pa) and the hydrophilic Laponite RD bath (τ_0 ~ 80 Pa) [15] can be calculated as approximately 10 μm (based on γ ~ 0.21 mN/m as seen

from **Supporting Information S2** and τ_0 ~ 20 Pa) and 500 μm, respectively. As a result, in aqueous support baths such as Laponite RD, the critical filament diameter is much larger due to the high interfacial tension, while in fumed silica bath PDMS filaments can have small diameters. When using a 100 μm diameter nozzle, the achievable minimum PDMS filaments can have the diameter of ~ 30 μm as observed and shown in **Figure S3a**, which is much smaller than that of the reported PDMS filament printed in an aqueous support bath [17]. The stability of filament morphology over time has been investigated and the results are illustrated in **Figure S3b**. Therefore, it is feasible to print PDMS structures with fine features using the fumed silica nanoparticle suspension-assisted 3D printing technique.

In extrusion-based 3D printing, filament dimeter is affected by both operating conditions such as dispensing pressure, nozzle diameter, and path speed as well as material rheological properties [31]. Herein, to print continuous filaments with various diameters, we investigate the effects of path speed and bath material concentration on the filament size. It is noted that when the other operating conditions are given, the relationship between filament diameter (D_f) and path speed (v_{path}) meets the following mathematical model due to the constant volume flow rate (Q): $D_f = \sqrt{\frac{4Q}{\pi v_{path}}}$. Thus, with the increase of path speed, the filament diameter decreases significantly first and then reduces slightly as shown in **Figure 2c**. In addition, the concentration of fumed silica bath can also affect filament diameter. With the increase of fumed silica concentration, the storage modulus in the support bath also increases as shown in **Figure 1e**, which makes the deposited liquid filaments undergo higher compression stress in the supporting bath, resulting in the decrease of filament diameter [19]. Using the current nozzle setup (200 μm in diameter), the achievable minimum diameter is approximately 50 μm as shown in **Figure 2c**.

3.4. Inter-filament fusion in fumed silica nanoparticle suspension. Except filament diameter and morphology, the fusion between adjacent filaments is another technical issue in extrusion-based 3D printing, which determines the surface roughness, dimensions and mechanical properties of printed structures significantly. Since fumed silica nanoparticle suspension-assisted 3D printing of hydrophobic inks also follows the "printing-then-solidification" procedure [15, 18, 20], in which printed 3D structures do not undergo solidification until the printing process is finished, the adjacent filaments can fuse well with each other at liquid state, resulting in the mechanical properties of printed structures similar to the casting ones [15, 18]. Thus, in this study the mechanical properties of printed PDMS structures are not investigated. In contrast, the effects of step distance on the sheet thickness and roughness are studied. **Figure 2d** illustrates the relationship between sheet thickness and step distance. Herein, the PDMS filaments with uniform diameter (D) of ~200 μm are deposited in the fumed silica bath and the step distance (d), distance between adjacent filaments, is increased from 100 μm to 225 μm with an interval of 25 μm, as illustrated in **Figure 2d-1**. As seen from **Figure 2d**, due to the volume constant the resulted sheet thickness (t) linearly decreases with the step distance/filament diameter ratio (d/D) as detailed in **Supporting Information S4**. In addition, when this step distance/filament diameter ratios are smaller than 1.0, the printed sheets have uniform surface (as shown in **Figure 2d-2**) with sheet thickness higher than one filament diameter (~200 μm), otherwise some gaps between adjacent filaments can be observed as shown in **Figure 2d-3** and the sheet thickness is close to the filament diameter.

Besides, the surface roughness of the sheets with various step distances are measured as shown in **Supporting Information S5**. From **Figure S5a** and **b**, we can find that the surface roughness of PDMS sheets with step distances between 125 and 175 μm presents no pronounced

variance (20.43 vs. 18.38 μm). In contrast, when the step distance is close to the filament diameter (~200 μm), the surface roughness increases to 25.06 μm. That is because in fumed silica nanoparticle suspension each deposited filament is held stably *in situ* and maintains at liquid state. Thus, the subsequently deposited filament can easily fuse well with the previously deposited filament and flatten the overlap region, resulting in a relatively smooth surface and a sheet thickness higher than a filament diameter as shown in **Figure S5c**. However, when the step distance is close to the filament diameter, the overlap region between adjacent filaments is too small to fill the gaps generated between two deposited filaments, which leads to a rougher surface and a thinner sheet thickness equivalent to the filament diameter.

3.5. PDMS structure printing in fumed silica nanoparticle suspension. Based on the printability knowledge from the filament formation and inter-filament fusion, complex PDMS structures are printed in fumed silica bath. First, a PDMS fluidic microchip (12.0 × 12.0 × 2.4 mm) with micro-scale channels is printed in a fumed silica bath as shown in the printing schematic in **Figure 3a**. PDMS base agent is mixed with a curing agent at a given ratio and loaded into the dispensing nozzle to print the fluidic microchip layer by layer as shown in **Movie M3**. After mixing with the curing agent, the PDMS base agent starts to cross-link gradually as explained in **Figure 3b** and the entire solidification period may take around 24 hours at room temperature. To improve the fabrication efficiency, the temperature of the fumed silica bath is increased to approximately 80 °C, and at this temperature the printed

PDMS structures may cross-link completely in only 40 minutes. Due to the thermal stability of the fumed silica bath at high temperatures as shown in **Figure 1h**, it maintains its yield-stress property around 80 °C and can stably hold the cross-linking PDMS structures *in situ* before the solidification process is complete.

The designed microchip has continuous micro-channels on the surface with a depth of 0.9 mm and a width of 0.5 mm as shown in **Figure 3c-1**. After heating in the fumed silica bath at 80 °C, the PDMS microchip is completely cross-linked and can be directly removed from the bath due to its mechanical robustness. After cleaning the residual fumed silica nanoparticle suspension on the surface and in the channels by water rushing, a silicone oil-based color dye is added in the printed channels to visualize the channel profile as shown in **Figure 3c-2**. **Figure 3c-3** shows the top view of part of the micro-channels. As seen from **Figure 3c-2** and **c-3**, the printed channels have a well-defined shape with clear boundaries. In addition, all the dimensions of the microchip are measured and compared with the designed chip as shown in **Supporting Information S6**, which proves the effectiveness of fumed silica support bath in PDMS-based microchip fabrication.

In addition to microchip structures, the fumed silica nanoparticle suspension can also be used as the support bath to facilitate 3D printing of other complex structures. Herein, a PDMS octopus-like structure (**Figure 3d-1**) is designed, which has overall dimensions of 42.0 × 42.0 × 32.0 mm. Due to the existence of many overhang sections, such an irregular PDMS structure is difficult to be fabricated by a conventional molding and/or casting approach. However, with the help of fumed silica bath we can easily print and cross-link the octopus-like structure as shown in **Figure 3d-2** and **d-3**. The comparison of the designed dimensions and measured ones are

detailed in **Supporting Information S7**, which verifies the printing accuracy of the fumed silica nanoparticle suspension-assisted 3D printing approach.

3.6. SU-8 structure printing in fumed silica nanoparticle suspension. In addition, fumed silica nanoparticle suspension can be utilized to print UV curable hydrophobic inks due to its excellent UV transparency as shown in **Figure 1g**. Negative photoresist SU-8 is selected as an exemplary ink material to be printed in the fumed silica support bath. Due to its high chemical and thermal resistances as well as good mechanical properties, SU-8 has been widely used in various fields including microelectromechanical systems (MEMS) [32] and microfluidic systems [33, 34], to name a few. However, due to the relatively long UV cross-linking time, the photomask-assisted polymerization approach is the most commonly used technique to fabricate SU-8 structures. Although 3D printing of SU-8 structures in a hydrophilic support bath (Laponite suspension) has been reported [15], due to the interfacial tension effect the deposited filaments usually have a larger diameter, resulting in the printed structures with low resolution. Thus, it is still a challenge to 3D print high-resolution complex structures with hydrophobic SU-8. By using the fumed silica nanoparticle suspension as the support bath, a printed SU-8 structure can retain its continuous shape in liquid during printing as shown in **Figure 4a**. After printing, UV radiation is used to solidify the SU-8 structure in the support bath, which makes the epoxide monomers of SU-8 be transformed from a low-molecular weight melt to a highly cross-linked network as shown in **Figure 4b**.

To prove the effectiveness of fumed silica nanoparticle suspension for SU-8 printing, an SU-8 filament is printed in a fumed silica bath first. The printed filament is kept in the bath for one hour without undergoing UV radiation and then imaged under microscope as shown in **Figure 4c-1**. From **Figure 4c-1**, it is observed that the printed SU-8 filament does not break up into

droplets in the observation window and presents a well-defined shape with clear boundaries. When another SU-8 filament is deposited adjacent to the previous one, they can fuse well with each other as shown in **Figure 4c-2**.

Then a SU-8 gear is designed as detailed in **Supporting Information S8** and printed in the fumed silica bath as shown in **Figure 4a-2**. After printing, the SU-8 gear is exposed under UV radiation for 15 minutes to cross-link and further solidified in an oven at temperature of 90 °C for 30 minutes as shown in **Figure 4b-2**. After that, the solidified SU-8 gear is collected from the fumed silica bath, and the residual fumed silica nanoparticle suspension is removed per the same protocol. The resulted fumed silica-free SU-8 gear is illustrated in the inset of **Figure 4d**. Finally, the gear is assembled with an axle connecting two wheels as shown in **Figure 4d**. The testing of the printed SU-8 gear is performed by driving a gear-fixed motor for 10 speed-up-and-down circles as shown in **Figure 4e**, and part of the process is recorded as **Movie M4**. After testing, the gear is disassembled from the axle and imaged optically to check the mechanical integrity, and part of its shape is shown in the inset of **Figure 4e**. Furthermore, the dimensions of the gear are measured and compared to those as designed as detailed in **Supporting Information S8**. As seen from **Figure 4e** and **Table S2**, there is no pronounced deformation and/or crack in the SU-8 gear after testing and its dimensions are close to the designed values. The mechanical integrity and dimensional match are attributed to the proposed printing-then-gelation mechanism, under which each deposited SU-8 filaments fuse well with each other to improve the interfacial strength, resulting in the excellent mechanical stiffness of the entire 3D structure.

3.7. Electronic component printing in fumed silica nanoparticle suspension. For further illustration, an epoxy-based silver conductive ink is used to print electronic components in a fumed silica bath. The schematic of the printing process is shown in **Figure 5a-1**. After mixing

the epoxy-based conductive ink (**Figure 5a-2**) with a hardener (**Figure 5a-3**), the cross-linking process occurs, and the epoxy monomers gradually connect with each other to form stable 3D molecular networks with the help of hardener polymer chains as shown in **Figure 5a-4**. It is noted that in the fumed silica bath the conductive ink cross-linking process may take approximately 10 days at room temperature. Thus, each deposited liquid conductive filament has enough time to fuse well with adjacent ones.

To investigate the effects of fabrication approach on the component resistance, rectangular-shaped samples are fabricated by both printing and casting. After cross-linking in the fumed silica nanoparticle suspension per the same protocol, the measured resistances are shown in **Figure 5b**. It is found that the measured resistance of cast samples is similar to that of printed samples, and the slightly higher resistance of 3D printed samples is attributed to some impurity defects during printing such as air bubbles and/or residual fumed silica nanoparticle suspensions entrapped between adjacent layers during printing.

Select electronic components are printed in the fumed silica bath. First, an inductor is designed as shown in the inset of **Figure 5c-1** and printed at liquid state in the fumed silica bath (**Figure 5c-1**). After keeping in the bath for 10 days, the inductor is solidified and can be collected from the bath. Then, the residual fumed silica nanoparticle suspensions are rinsed from the surface and the solid fumed silica-free inductor is illustrated in **Figure 5c-2**. The excellent conductivity of the 3D printed inductor is verified by connecting it in series with a light-emitting diode (LED) light and a direct current power supply, where the inductor functions as a conductive wire as shown in **Movie M5**. In addition, this 3D printed inductor can also be used as a solenoid. As shown in **Figure 5c-3**, the charged inductor can generate a magnetic field to move/rotate the needle of a compass (**Movie M5**). When the electric current is turned off, the

magnetic field vanishes, and the needle moves back to the original position as shown in **Figure 5c-4**. Such solenoids can be further utilized to make some complex devices such as transducers, relays, and solenoid valves for future applications. Besides inductors, other complex structures such as battery anode/cathode sets can also be printed in the fumed silica nanoparticle suspension as shown in **Figure 5d-2**. Per the same solidification and post-treatment protocol, the fumed silica-free structures are illustrated in **Figure 5d-3**. The dimensions of the designed and fabricated electronic components at different measurement windows (including immediately after printing, 10-day after printing, and after residual fumed silica rinsing) are summarized in **Supporting Information S9**. From **Table S3**, it is found that the sizes of the electronic components on Day 10 are slightly larger than those on Day 0, which may be attributed to the slow diffusion of epoxy monomers into the fumed silica bath, resulting in the swollen profiles when measured in the bath. However, during rinsing these uncross-linked conductive monomers are removed with the residual fumed silica nanoparticle suspensions on the surface of the electronic components, which leads to the decrease of the measured dimensions.

4. CONCLUSIONS

In summary, we propose the fumed silica-mineral oil suspension as a versatile support bath to facilitate 3D printing of hydrophobic inks. Due to the hydrophobic property of the proposed support bath, the interfacial tension effect between bath and ink materials is negligible, which makes it feasible to print PDMS filaments with a much better resolution of 30 μm. In addition, the excellent UV transparency and thermal stability of the fumed silica nanoparticle suspension enable it to be used as the support bath for UV curable and/or thermal cross-linking hydrophobic ink printing. For demonstration, three hydrophobic inks, including PDMS to show the silicone

oil printability and *in situ* curing at a high temperature (80ºC), SU-8 to demonstrate the printing of UV curable oily resin inks, and epoxy-based conductive ink to test the printing of oily resin inks, are used to fabricate various complex 3D structures.

It should be noted that due to its stable chemical property and ecologically safe property, the fumed silica-mineral oil suspension can be repeatedly used in 3D printing of hydrophobic inks and/or disposed as a nontoxic material. In addition to the fumed silica-mineral oil suspension, the fumed silica can be prepared as an aqueous suspension for printing of hydrophilic materials. Since it is not of interest herein, it is not explored in this study.

Future work may study the solid-liquid transition of fumed silica nanoparticle suspensions, investigate the effect of interfacial tension on the filament formation and/or morphology in the fumed silica-mineral oil support bath based on the Plateau-Rayleigh instability model, which may help to understand the underlying printing physics, and utilize the proposed fumed silica nanoparticle suspension-assisted 3D printing technique to fabricate more complex structures for some practical applications.

ACKNOWLEDGEMENTS

This research was partially supported by the US National Science Foundation (CMMI-1762941). Y. J., K. S., and Y. H. thank Anton Paar for its rheological testing facilities at the University of Florida as well as Karen Kelley and Kimberly Backer-Kelley of the Interdisciplinary Center for Biotechnology Research (ICBR) at the University of Florida for their efforts in SEM and TEM imaging.

SUPPORTING INFORMATION

Supporting Information is available free of charge from the ACS Applied Materials & Interfaces home page (http://pubs.acs.org/journal/aamick).

Supporting Information S1: PDMS filament printing in hydrophilic and hydrophobic baths. (PDF)

Supporting Information S2: Investigation of interfacial tension effects. (PDF)

Supporting Information S3: Achievable minimum diameter of PDMS filaments and their stability over time. (PDF)

Supporting Information S4: Mathematical model between step distance and sheet thickness. (PDF)

Supporting Information S5: Surface roughness measurement and inter-filament bonding formation. (PDF)

Supporting Information S6: Comparison of the 3D microchip model and 3D printed microchip. (PDF)

Supporting Information S7: Comparison of the 3D octopus model and 3D printed octopus-like structure. (PDF)

Supporting Information S8: Design and dimensional measurements of SU-8 gear. (PDF)

Supporting Information S9: Dimensional measurements of electronic components over time. (PDF)

Supporting Information M1: Filament printing in fumed silica bath. (Movie)

Supporting Information M2: Interfacial tension measurements in different medium. (Movie)

Supporting Information M3: PDMS microchip printing in fumed silica bath. (Movie)

Supporting Information M4: SU-8 gear testing. (Movie)

Supporting Information M5: Epoxy-based inductor testing. (Movie)

AUTHOR CONTRIBUTIONS

Y. J., N. G., and Y. H. conceived the concept of this work, Y. J. and K. S. conducted the experiments and analysis, and Y. J. and Y. H. wrote the manuscript.

COMPETING FINANCIAL INTERESTS

There are no competing financial interests.

REFERENCES

1. Bartlett, N. W.; Tolley, M. T.; Overvelde, J. T.; Weaver, J. C.; Mosadegh, B.; Bertoldi, K.; Whitesides, G. M.; Wood, R. J. A 3D-Printed, Functionally Graded Soft Robot Powered by Combustion. *Science* **2015,** *349,* 161-165.
2. Wehner, M.; Truby, R. L.; Fitzgerald, D. J.; Mosadegh, B.; Whitesides, G. M.; Lewis, J. A.; Wood, R. J. An Integrated Design and Fabrication Strategy for Entirely Soft, Autonomous Robots. *Nature* **2016,** *536,* 451-455.
3. Schaffner, M.; Faber, J. A.; Pianegonda, L.; Rühs, P. A.; Coulter, F.; Studart, A. R. 3D Printing of Robotic Soft Actuators with Programmable Bioinspired Architectures. *Nature Communications* **2018,** *9,* 878.
4. Kong, Y. L.; Tamargo, I. A.; Kim, H.; Johnson, B. N.; Gupta, M. K.; Koh, T. W.; Chin, H. A.; Steingart, D. A.; Rand, B. P.; McAlpine, M. C. 3D Printed Quantum Dot Light-Emitting Diodes. *Nano Letters* **2014,** *14,* 7017-7023.

5. Muth, J. T.; Vogt, D. M.; Truby, R. L.; Mengüç, Y.; Kolesky, D. B.; Wood, R. J.; Lewis, J. A. Embedded 3D Printing of Strain Sensors within Highly Stretchable Elastomers. *Advanced Materials* **2014,** *26,* 6307-6312.

6. Valentine, A. D.; Busbee, T. A.; Boley, J. W.; Raney, J. R.; Chortos, A.; Kotikian, A.; Berrigan, J. D.; Durstock, M. F.; Lewis, J. A. Hybrid 3D Printing of Soft Electronics. *Advanced Materials* **2017,** *29,* 1703817.

7. Calleja, M.; Tamayo, J.; Johansson, A.; Rasmussen, P.; Lechuga, L. M.; Boisen, A. Polymeric Cantilever Arrays for Biosensing Applications. *Sensor Letters* **2003,** *1,* 20-24.

8. Eckel, Z. C.; Zhou, C.; Martin, J. H.; Jacobsen, A. J.; Carter, W. B.; Schaedler, T. A. Additive Manufacturing of Polymer-Derived Ceramics. *Science* **2016,** *351,* 58-62.

9. Huang, Y.; Leu. M. C.; Mazumder, J.; Donmez, A. Additive Manufacturing: Current State, Future Potential, Gaps and Needs, and Recommendations. *ASME Journal of Manufacturing Science and Engineering* **2015,** *137,* 014001.

10. Huang, Y.; Schmid, S. Additive Manufacturing for Health: State of the Art, Gaps and Needs, and Recommendations. *ASME Journal of Manufacturing Science and Engineering* **2018,** *140,* 094001.

11. Ahn, B. Y.; Duoss, E. B.; Motala, M. J.; Guo, X.; Park, S. I.; Xiong, Y.; Yoon, J.; Nuzzo, R. G.; Rogers, J. A.; Lewis, J. A. Omnidirectional Printing of Flexible, Stretchable, and Spanning Silver Microelectrodes. *Science* **2009,** *323,* 1590-1593.

12. Sun, K.; Wei, T. S.; Ahn, B. Y.; Seo, J. Y.; Dillon, S. J.; Lewis, J. A. 3D Printing of Interdigitated Li-Ion Microbattery Architectures. *Advanced Materials* **2013,** *25,* 4539-4543.

13. Compton, B. G.; Lewis, J. A. 3D-Printing of Lightweight Cellular Composites. *Advanced Materials* **2014,** *26,* 5930-5935.

14. Jin, Y.; Liu, C.; Chai, W.; Compaan, A.; Huang, Y. Self-Supporting Nanoclay as Internal Scaffold Material for Direct Printing of Soft Hydrogel Composite Structures in Air. *ACS Applied Materials & Interfaces* **2017,** *9,* 17456-17465.

15. Jin, Y.; Compaan, A.; Chai, W.; Huang, Y. Functional Nanoclay Suspension for Printing-then-Solidification of Liquid Materials. *ACS Applied Materials & Interfaces* **2017,** *9,* 20057-20066.

16. Bhattacharjee, T.; Zehnder, S. M.; Rowe, K. G.; Jain, S.; Nixon, R. M.; Sawyer, W. G.; Angelini, T. E. Writing in the Granular Gel Medium. *Science Advances* **2015,** *1,* e1500655.

17. Hinton, T. J.; Hudson, A.; Pusch, K.; Lee, A.; Feinberg, A. W. 3D Printing PDMS Elastomer in a Hydrophilic Support Bath via Freeform Reversible Embedding. *ACS Biomaterials Science & Engineering* **2016,** *2,* 1781-1786.

18. Jin, Y.; Compaan, A.; Bhattacharjee, T.; Huang, Y. Granular Gel Support-Enabled Extrusion of Three-Dimensional Alginate and Cellular Structures. *Biofabrication* **2016,** *8,* 025016.

19. Jin, Y.; Chai, W.; Huang, Y. Printability Study of Hydrogel Solution Extrusion in Nanoclay Yield-Stress Bath during Printing-then-Gelation Biofabrication. *Materials Science and Engineering: C* **2017,** *80,* 313-325.

20. Jin, Y.; Chai, W.; Huang, Y. Fabrication of Stand-Alone Cell-Laden Collagen Vascular Network Scaffolds Using Fugitive Pattern-Based Printing-then-Casting Approach. *ACS Applied Materials & Interfaces* **2018,** *10,* 28361-28371.

21. Hinton, T. J.; Jallerat, Q.; Palchesko, R. N.; Park, J. H.; Grodzicki, M. S.; Shue, H. J.; Ramadan, M. H.; Hudson, A. R.; Feinberg, A. W. Three-Dimensional Printing of Complex Biological Structures by Freeform Reversible Embedding of Suspended Hydrogels. *Science Advances* **2015,** *1,* e1500758.

22. O'Bryan, C. S.; Bhattacharjee, T.; Hart, S.; Kabb, C. P.; Schulze, K. D.; Chilakala, I.; Sumerlin, B. S.; Sawyer, W. G.; Angelini, T. E. Self-Assembled Micro-Organogels for 3D Printing Silicone Structures. *Science Advances* **2017,** *3,* e1602800.

23. Khan, S. A.; Zoeller, N. J. Dynamic Rheological Behavior of Flocculated Fumed Silica Suspensions. *Journal of Rheology* **1993,** *37,* 1225-1235.

24. Raghavan, S. R.; Khan, S. A. Shear-Induced Microstructural Changes in Flocculated Suspensions of Fumed Silica. *Journal of Rheology* **1995,** *39,* 1311-1325.

25. Gong, S.; Schwalb, W.; Wang, Y.; Chen, Y.; Tang, Y.; Si, J.; Shirinzadeh, B.; Cheng, W. A Wearable and Highly Sensitive Pressure Sensor with Ultrathin Gold Nanowires. *Nature Communications* **2014,** *5,* 3132.

26. Huh, D.; Matthews, B. D.; Mammoto, A.; Montoya-Zavala, M.; Hsin, H. Y.; Ingber, D. E. Reconstituting Organ-Level Lung Functions on a Chip. *Science* **2010,** *328,* 1662-1668.

27. Mata, A.; Fleischman, A. J.; Roy, S. Characterization of Polydimethylsiloxane (PDMS) Properties for Biomedical Micro/Nanosystems. *Biomedical Microdevices* **2005,** *7,* 281-293.

28. Andreas, J. M.; Hauser, E. A.; Tucker, W. B. Boundary Tension by Pendant Drops. *The Journal of Physical Chemistry* **1938,** *42,* 1001-1019.

29. Freer, E. M.; Wong, H.; Radke, C. J. Oscillating Drop/Bubble Tensiometry: Effect of Viscous Forces on the Measurement of Interfacial Tension. *Journal of Colloid and Interface Science* **2005,** *282,* 128-132

30. Ismail, A. E.; Grest, G. S.; Heine, D. R.; Stevens, M. J.; Tsige, M. Interfacial Structure and Dynamics of Siloxane Systems: PDMS-Vapor and PDMS-Water. *Macromolecules* **2009,** *42,* 3186-3194.

31. Zhang, Z.; Jin, Y.; Yin, J.; Xu, C.; Xiong, R.; Christensen, K.; Ringeisen, B. R.; Chrisey, D. B.; Huang, Y. Evaluation of Bioink Printability for Bioprinting Applications. *Applied Physics Review* **2018,** *5,* 041304.

32. Lorenz, H.; Despont, M.; Fahrni, N.; LaBianca, N.; Renaud, P.; Vettiger, P. SU-8: A Low-Cost Negative Resist for MEMS. *Journal of Micromechanics and Microengineering* **1997,** *7,* 121.

33. Zhang, J.; Tan, K. L.; Hong, G. D.; Yang, L. J.; Gong, H. Q. Polymerization Optimization of SU-8 Photoresist and Its Applications in Microfluidic Systems and MEMS. *Journal of Micromechanics and Microengineering* **2001,** *11,* 20.

34. Lin, C. H.; Lee, G. B.; Chang, B. W.; Chang, G. L. A New Fabrication Process for Ultra-Thick Microfluidic Microstructures Utilizing SU-8 Photoresist. *Journal of Micromechanics and Microengineering* **2002,** *12,* 590.

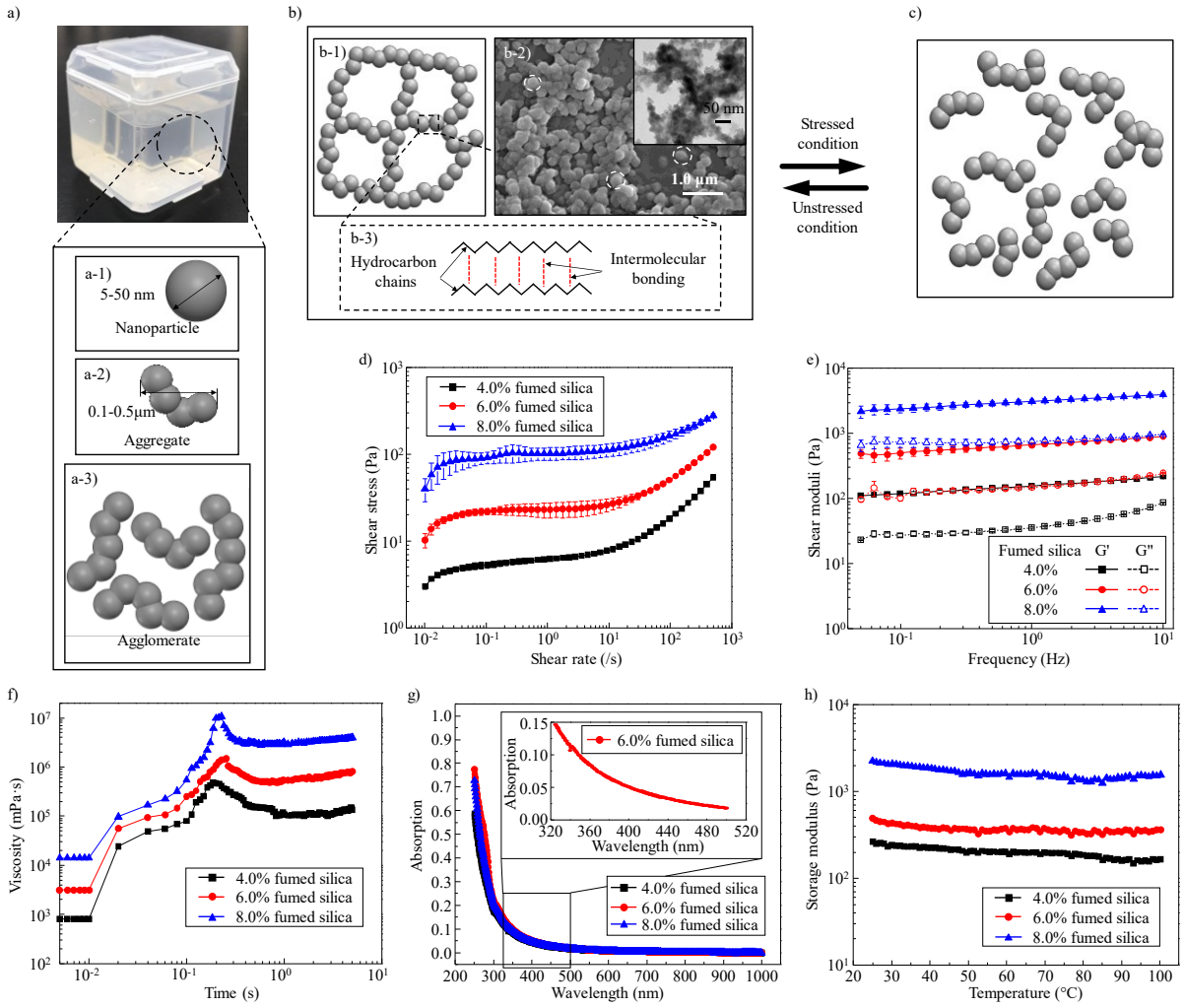

Figure 1. Characterization of fumed silica nanoparticle suspension. a) Prepared transparent fumed silica-mineral oil suspension and schematics of a-1) nanoparticle, a-2) aggregate, and a-3) agglomerate in fumed silica nanoparticle suspension. b) Microstructures of fumed silica nanoparticle suspension upon unstressed condition: b-1) schematic of the stable 3D networked microstructures, b-2) SEM image and TEM image (inset) of fumed silica nanoparticle suspension, and b-3) schematic of the intermolecular bonds between adjacent fumed silica aggregates. c) Schematic of the microstructures of fumed silica nanoparticle suspension up stressed condition. Rheological properties of fumed silica nanoparticle suspensions at different concentrations: d) shear stress as a function of shear rate, e) shear moduli as a function of frequency, and f) viscosity as a function of testing time. g) UV transparency of fumed silica nanoparticle suspensions at different concentrations. h) Thermal stability of fumed silica nanoparticle suspensions in temperature range of 25-100 °C. Error bars: plus/minus one standard deviation.

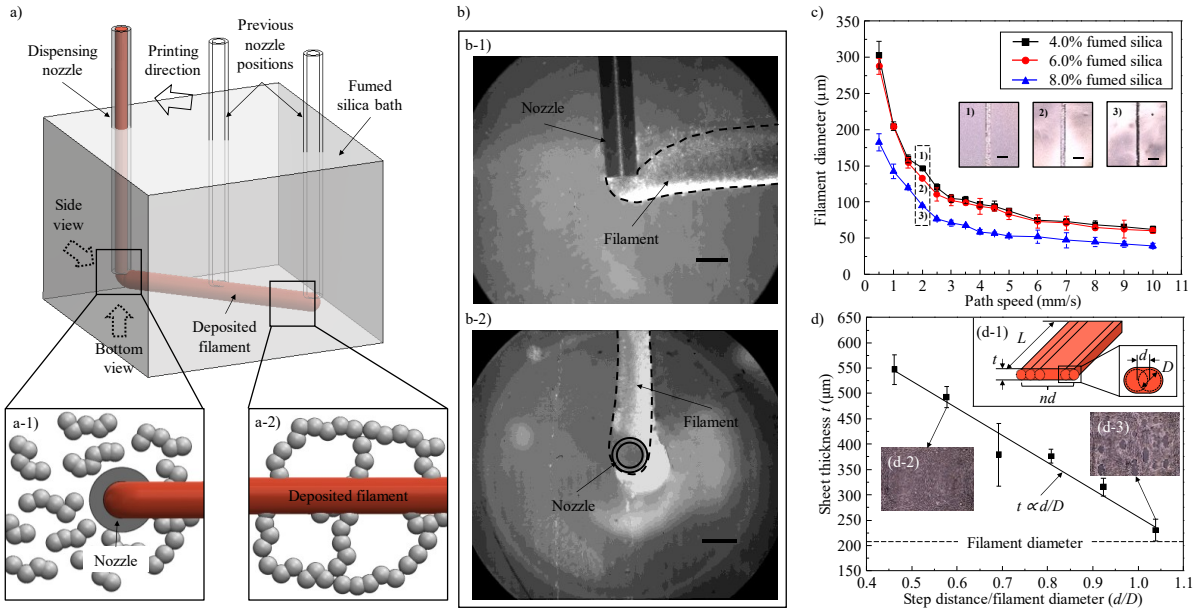

Figure 2. Filament/sheet printing in fumed silica bath. a) Schematic of 3D printing of hydrophobic inks in fumed silica bath. b-1) Side and b-2) bottom views of filament printing process in fumed silica bath (profile of printed filament is marked by dash lines). c) Filament diameter as a function of path speed. d) Sheet thickness as a function of step distance/filament diameter ratio. Scale bars: 1.0 mm for (b-1) and b-2)) and 0.5 mm for c), and error bars: plus/minus one standard deviation.

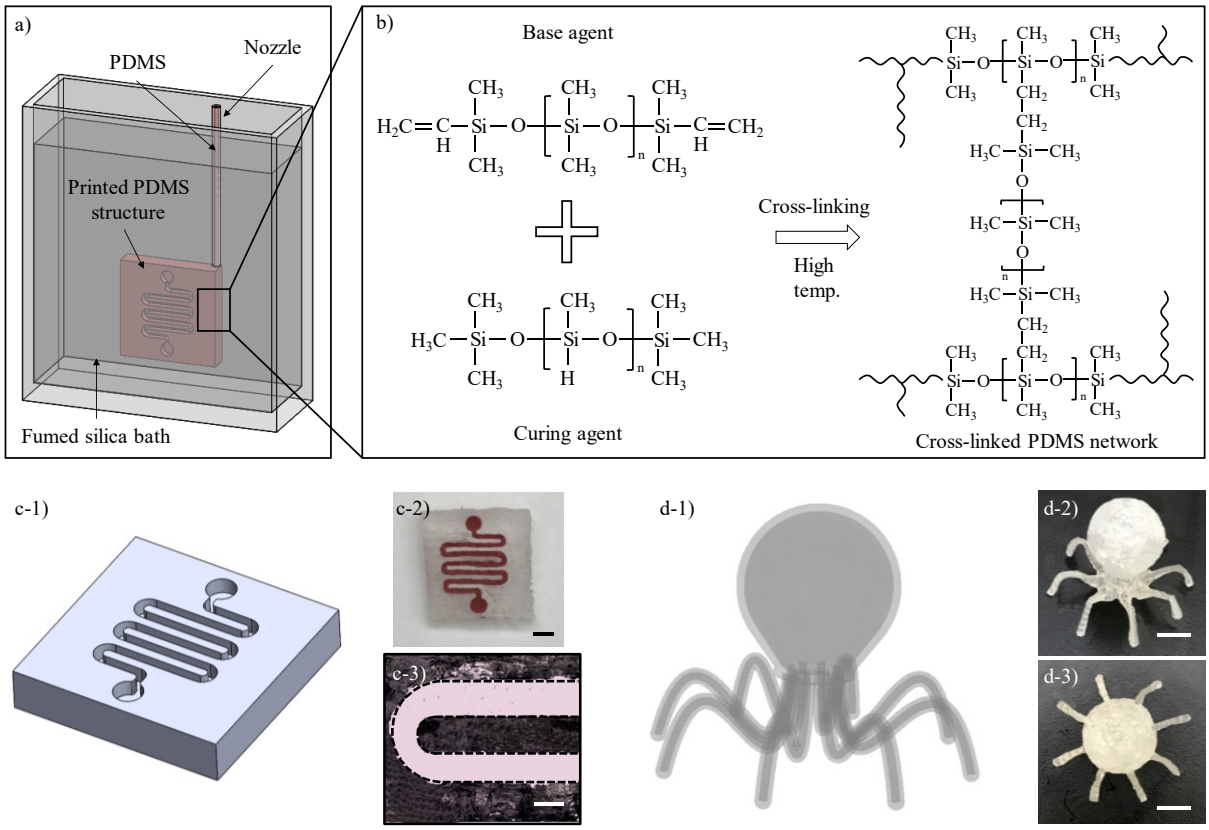

Figure 3. PDMS structures printing in fumed silica bath. a) Schematic of printing PDMS structure in fumed silica bath. b) Schematic of PDMS cross-linking mechanism. c) PDMS fluidic microchip design and fabrication: c-1) schematic of PDMS chip, c-2) printed PDMS chip with micro-channels filled with a red-color solution, and c-3) zoom-in image of a micro-channel. d) PDMS octopus design and fabrication: d-1) schematic of PDMS octopus, d-2) global and d-3) top views of the printed PDMS octopus. Scale bars: 2.0 mm for c-1), 0.5 mm for c-2), and 10.0 mm for d).

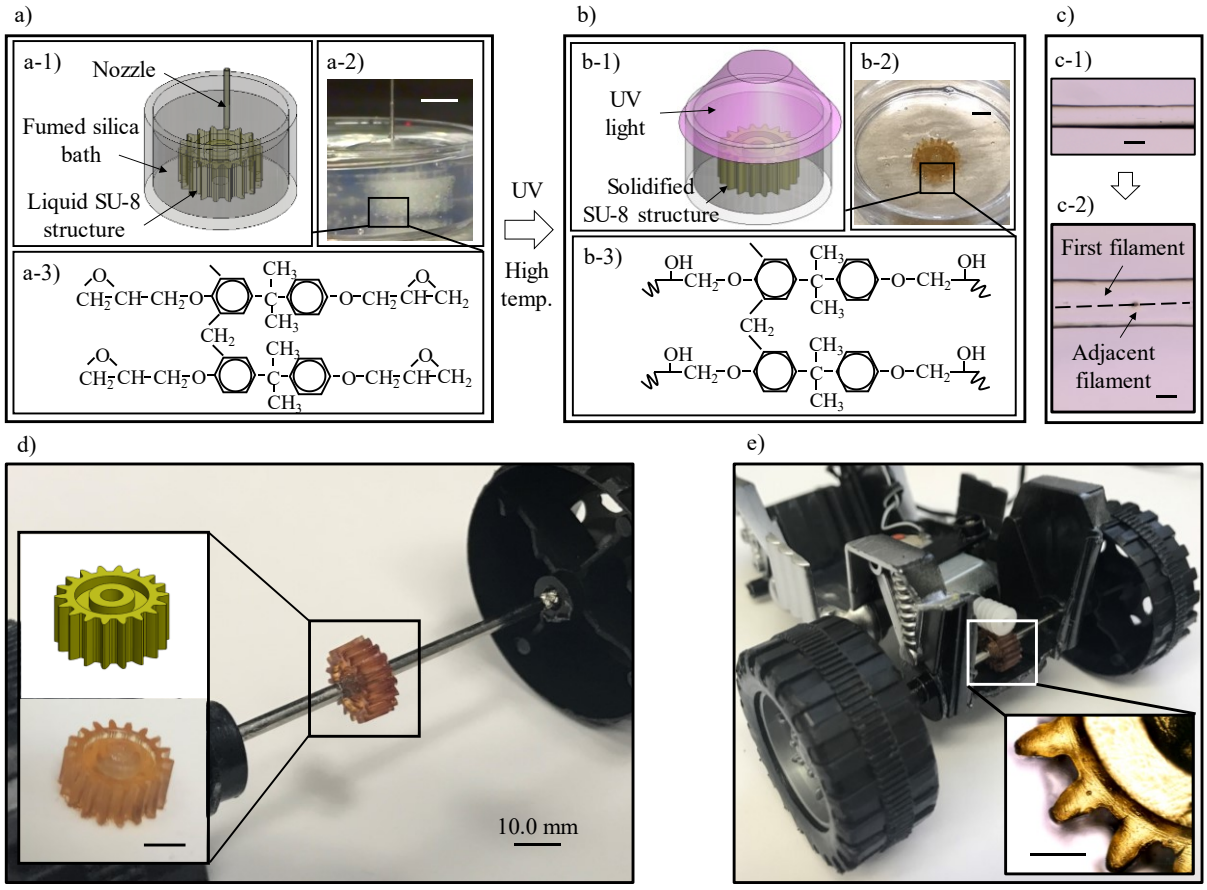

Figure 4. SU-8 structure printing in fumed silica bath. a) Schematic of SU-8 structure printing in fumed silica bath. b) Schematic of SU-8 structure cross-linking by UV radiation in fumed silica bath. c) Printing and fusion of adjacent SU-8 filaments in support bath. d) Fabricated SU-8 gear and its assembly (insets: designed and 3D printed SU-8 gears). e) Testing of printed SU-8 gear in gear sets (inset: image of tested SU-8 gear). Scale bars: 4.0 mm for a), b) and d), 0.2 mm for c), and 2.0 mm for e).

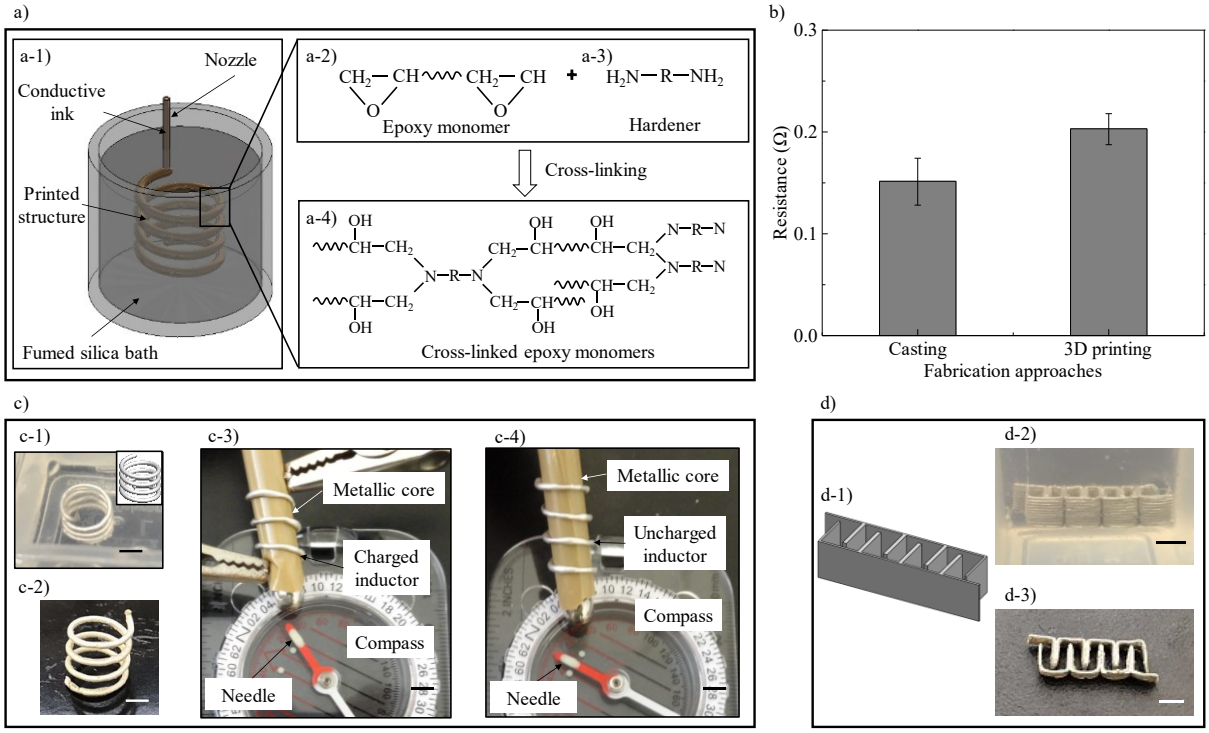

Figure 5. Conductive ink printing in fumed silica bath. a) Schematics of conductive ink printing and cross-linking in fumed silica bath. b) Comparison of resistance between conductive samples fabricated by casting and fumed silica nanoparticle suspension-assisted printing. c) Conductive inductor fabrication and application: c-1) the inductor printing in the fumed silica bath, c-2) the inductor after rinsing the residual fumed silica nanoparticle suspension, and the application of the inductor as a solenoid in c-3) charged and c-4) uncharged states. d) Battery anode/cathode set design and fabrication. Scale bars: 4.0 mm, and error bars: plus/minus one standard deviation.

Table of Contents Graph

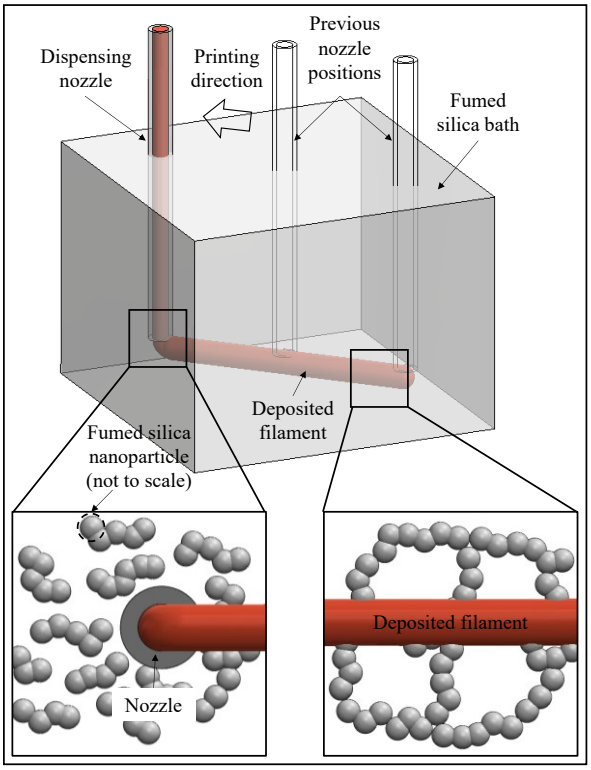

Fumed silica-mineral oil suspension used as a hydrophobic yield-stress support bath

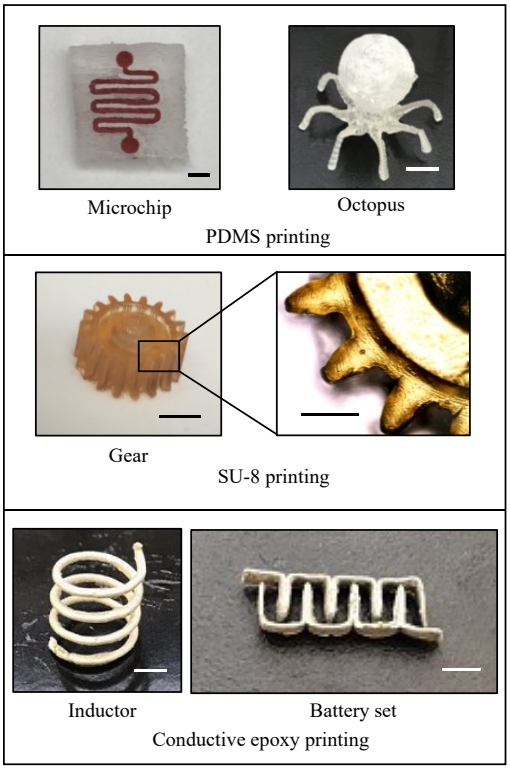

Printing of various hydrophobic inks in hydrophobic fumed silica support bath